Impact of the electron environment on the lifetime of the $^{229}Th^{m}$ low-lying isomer

F. F. Karpeshin[1] and M. B. Trzhaskovskaya[2]
[1]*Institute of Physics, St. Petersburg State University, St. Petersburg, Russia*
[2]*Petersburg Nuclear Physics Institute, Gatchina, Russia*
(Received 3 May 2007; published 15 November 2007)

The question of the lifetime of the $^{229}Th^{m}$ low-lying isomer is considered in light of current experimental research. A strong effect of the electron shell on lifetime is demonstrated, depending on the energy of the isomer. Calculations are performed within the framework of the multiconfiguration Dirac-Fock method. The calculated lifetime ranges from around 1 min down to 10^{-5} s. Prospects for further experimental research of the isomer are discussed.

DOI: 10.1103/PhysRevC.76.054313 PACS number(s): 23.20.Nx, 27.90.+b, 21.10.Tg

I. INTRODUCTION

The availability of new experimental facilities provides new opportunities for observing processes that occur comparatively rarely in neutral atoms under ordinary conditions [1,2]. Bound internal conversion (BIC) [3], where the conversion electron is lifted up to a bound state of the atom, is an example of such a process. The sharp resonance character of BIC, which is also known as resonance conversion, offers a way of accelerating nuclear processes by tuning the atomic frequencies in the field of a laser [4–7]. BIC was experimentally discovered in highly charged ions of $^{125}Te^{m}$ [3]. It was expected that the rate of the 35492 eV $M1$ transition should essentially retard in the ions of charge $q = 45$ and 46, when the binding energy of the $1s$ electron exceeds the conversion threshold. Surprisingly, the experiment showed that the lifetime held, which was interpreted as a manifestation of BIC. The retention of the conversion rate when crossing the continuum boundary was confirmed analytically in the general case [3]. Calculations performed in the framework of the Dirac-Fock (DF) method are in agreement with the experimental data [8]. In Ref. [9], the shift of the x-ray line predicted in Ref. [3] was experimentally confirmed.

Another important example of BIC is provided by the decay of the isomer of $^{229}Th^{m}$, which occurs at a uniquely low energy within 10 eV. For a long time, the most accepted value has been $\omega_n = 3.5 \pm 1$ eV [10]. This energy is below the threshold of traditional internal conversion (IC) because, according to our calculation, the binding energy ε_{7s} of the valence $7s$ electron in the Th atom (ionization potential) is equal to $I = 5.2$ eV. The previous recommendation of Reich and Helmer was $\omega_n = -1 \pm 4$ eV [11]. Other measurements led to the value of 5.5 ± 1 eV [12]. The last reported value, obtained using a detector with better resolution, is 7.6 ± 0.5 eV [13]. However, despite a great number of repeated attempts [14–19], nobody observed direct decay of the isomer in question with confidence, since a precision determination of the few eV energy difference on the background of tens keV transition energies is a very difficult task. For this reason, we do not confine the calculation by considering a particular nuclear energy, but rather we investigate the problem of the lifetime generally. We also consider the possible influence of both traditional IC and BIC on the lifetime of the isomer.

The study of the $^{229}Th^{m}$ isomer attracts particular interest specifically because of the chance to discover a new physics related to the resonance atomic-nuclear interactions, which enables, e.g., population inversion of the ground and excited levels [20]. The traditional channels of isomer deexcitation are the radiative and α decays. The aim of experiments used to be the detection of soft photons from direct nuclear decay with an energy of around 3.5 eV. Moreover, a rather long lifetime of tens of hours was usually assumed in the experiments based on the Weisskopf estimation (cf. Refs. [14,21]). That was in spite of confident theoretical predictions that the lifetime of the isomer is much shorter in view of internal conversion processes, which drastically changes the nuclear lifetimes, especially at the transition energies near threshold [6,22,23]. It does not matter even if traditional IC turns out to be energetically forbidden, because there arises a number of decay channels through BIC according to the resonance electron bridge scheme. Similar to the case of $^{125}Te^{m}$, they take the place of traditional IC. In BIC, the electron is lifted up virtually to a higher lying discrete level, mainly $7s \rightarrow 8s$. From the $8s$ level, the electron returns to the $7s$ state via a cascade of two or more radiative transitions. Nuclear energy is thus taken off by several soft delayed photons.

Figure 1 demonstrates the Feynman graphs for the deexcitation of the isomer via (a) radiative decay and (b) BIC mechanisms. It has been shown in Refs. [20,21,24] within the one-electron DF method that BIC turns out to be the predominant decay mode in the case of the 3.5 eV energy of $^{229}Th^{m}$. The most probable chain of electron transitions is $7s \rightarrow 8s \rightarrow 7p \rightarrow 7s$. This is accompanied by the emission of two electric dipole photons, each with an energy of about $\omega_n/2$ [20,25]. The resonance conversion factor $\mathcal{R}$ is defined by the ratio of the BIC and radiative transition probabilities. The factor $\mathcal{R}$ is similar to the internal conversion coefficient (ICC) in the case of traditional IC. For the 3.5 eV $^{229}Th^{m}$ isomer, $\mathcal{R}$ appears to be one to three orders of magnitude, depending on the defect of resonance [21]. Therefore, the resonance electron bridge reduces the expected isomer lifetime to about 1 min or less. Moreover, it was noted that in the case of an accident resonance, the lifetime may be reduced to a small fraction of a second, down to 10^{-11} s [19].

Fresh opportunities for the BIC study were produced by Refs. [8,26] which took into account the residual interaction of electrons. This results in splitting of the atomic energy levels in the total angular momentum which increases the level

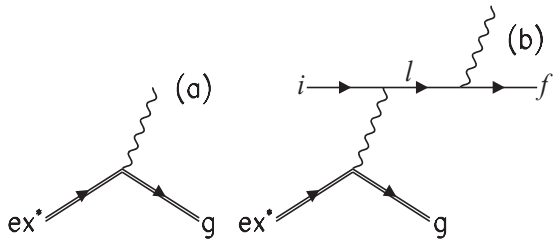

FIG. 1. Feynman graphs for the decay of the isomer via (a) the radiative decay and (b) BIC mechanisms. The ground and excited states of the nucleus are denoted by g and ex^*, respectively. The initial, intermediate, and final atomic states are denoted by i, ℓ, and f, respectively.

density and therefore, the probability of overlapping with the nuclear transition energy. In studies of the $M1$ transition in highly charged ions of $^{125}Te^m$ [8], allowance was made for the interaction between electrons of open shells in the framework of the multiconfiguration Dirac-Fock (MCDF) method [27]. In addition, the Breit magnetic interaction between atomic electrons and higher QED corrections to the atomic energy levels were considered. The calculations, while involving a modest set of basis configurations, revealed a considerable influence of the residual interactions on the factor $\mathcal{R}$. As mentioned above, the calculated lifetime of the $^{125}Te^m$ was in agreement with the experiment.

In the present paper, calculations for $^{229}Th^m$ are also carried out in the framework of the MCDF method. We extend the atomic basis essentially, including a number of the electron configurations. The Breit magnetic interaction is taken into account. We used in the calculations the RAINE package of computer codes [28]. Correspondingly, Sec. II is devoted to a consideration of the ICC for overthreshold energies. In Sec. III, we extend the BIC theory to take into account a great number of the intermediate and final electron states. We derive general expressions for the resonance conversion factor and for the spectra of primary and secondary photons. In Sec. IV, we discuss the results obtained, with respect to the prospective experimental research.

II. INTERNAL CONVERSION

Let us start from the latest value for the isomer energy, $\omega_n = 7.6 \pm 0.5$ eV [13]. In this case $\omega_n > I$, and the main channel of deexcitation is via traditional IC. Calculation of ICC near the very threshold is a challenging task. The results are sensitive to the atomic model.

The ICC calculation was performed in the first nonvanishing order of the perturbation theory using a spherically symmetric atomic potential of the free neutral atom of thorium. Electron wave functions were calculated in the framework of the relativistic Dirac-Fock method with the appropriate consideration of the exchange terms. The finite size of the nucleus was taken into consideration using the surface-current model [29] in which the penetration effect into the nucleus was approximately taken into account.

To test the accuracy of the theoretical model described above, a detailed comparison between experimental and theoretical values of ICCs was made in Refs. [30–32]. As was shown, the model allows one to obtain theoretical ICCs which agree with experimental values at the $\lesssim 1\%$ level both on average (for 100 experimental ICCs having uncertainties $\leqslant 5\%$) [30] and for specific nuclear transitions [31,32].

We calculated the ICC in the valence $7s$ shell which gives the predominant contribution to the total internal conversion rate in the case of the $M1$ transition at the threshold [25], as the state has maximal electron density at the origin. Note that there exists the problem of allowing for the hole in the atomic shell after conversion, which is being currently discussed (see, for example, Ref. [32] and references therein). For this reason, we present calculations for three cases [30]: (i) the hole is disregarded, that is, the electron wave functions for the bound and continuum states are calculated in the same atomic field of the neutral atom; (ii) the hole is taken into account using the self-consistent field (SCF) approximation, that is, the continuum wave function is calculated in the self-consistent field of the relevant ion; and (iii) the hole is taken into account within the frozen orbital (FO) approximation when the continuum wave function is also calculated in the ion field, but this field is constructed using the bound wave functions of the neutral atom.

The results are presented in Fig. 2 for transition energies up to 10 eV. As one can see from the figure, the calculated values vary by an order of magnitude within this domain. Their variation, depend on the model, reaches $\sim 50\%$ near the very threshold; however, it does not change the order of magnitude of the ICC. At the transition energy of 7.6 eV, the ICC value is about $\alpha^{M1} \approx 10^9$.

Now, based on the calculated value of ICC $\alpha^{M1} \approx 10^9$, we can estimate the isomer lifetime. The Weisskopf estimation for the $M1$ transition with the energy of 7.6 eV gives ~ 1 min [6]. Taking into account the hindrance factor of ~ 300, typical for

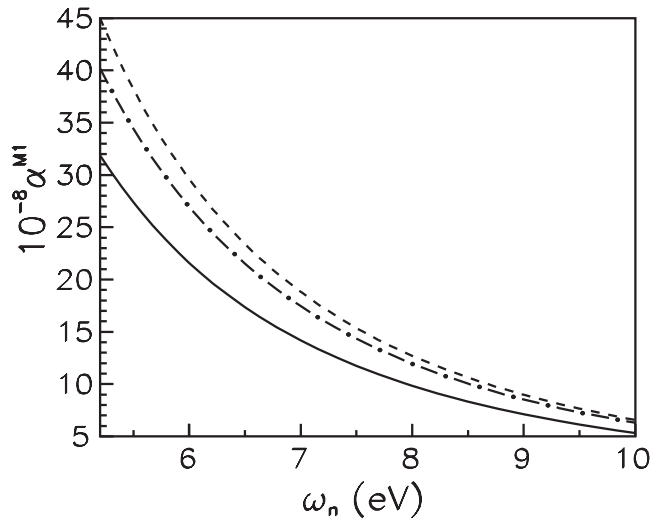

FIG. 2. ICC α^{M1}_{7s} multiplied by the factor 10^{-8} for the $7s$ shell of the Th atom for the transition energy near the threshold. Calculations were made without regard for the hole in the $7s$ shell after conversion (solid line), with regard for the hole in the FO approximation (dashed line), and with regard for the hole in the SCF approximation (dot-dashed line).

this domain of nuclei, with this value of ICC we arrive at the lifetime of the isomer of the order of $\sim 10^{-5}$ s.

III. BIC WITH REGARD TO CONFIGURATION MIXING

Let us examine the case $\omega_n < I$. If the energy around 5.5 eV is accepted [12], we turn out to be just on the border of the continuum. This makes calculation a tedious problem, as the result is determined by the interplay of the values of ω_n and I within the domain of ~ 1 eV. On physical grounds, however, with the results of Ref. [3], one can predict that ICC α^{M1} smoothly goes over $\mathcal{R}$, the BIC factor, as ω_n crosses the boundary. Therefore, the value of ICC (above threshold) or $\mathcal{R}$ (below threshold) is expected to be approximately 3×10^9 (see Fig. 2). Correspondingly, the lifetime is expected to be of the order of 1.6×10^{-5} s.

Physics becomes considerably richer when ω_n further decreases. The case $\omega_n = 3.5 \pm 1$ eV [10] was studied in Refs. [21,24,33], where it was shown that the interaction of configurations is of great importance for the lifetime of the isomer, which is determined by the $\mathcal{R}$ factor. The interplay of the two main effects of the configuration mixing was noted as (1) the line strength becomes fragmented, which damps the resonance, and (2) BIC becomes more regular and is less sensitive to the energies of particular levels.

Herein we extend the basis of the electron configurations essentially. This allows us to derive even more definite conclusions about the fragmentation strength than obtained in Ref. [33] and to correct inaccuracies that occurred therein. Also for the sake of completeness, we cite in Tables I–III results obtained with configuration sets 1–7 [33], along with results of the present calculation with configuration set 8.

Interaction of configurations can be classified into three kinds. In Fig. 3, the Feynman graphs represent (a) the interaction arising due to one-electron mixing described by operators of the kinetic energy and the Coulomb field of the nucleus, (b) the two-electron interaction through the mean field of the atom, and (c) the two-electron interaction with more complicated many-electron configurations. All the interactions turn out to be essential in the BIC consideration [8,26]. So we derive below expressions for the resonance conversion factor $\mathcal{R}$ taking into account the residual interactions.

The diagram in Fig. 1(b) was first considered in Ref. [34] for the nonradiative muon transfer in prompt-fission fragments. It was shown in Ref. [33] that the probability $\Gamma_{\rm BIC}^{(i\to f)}$ of the $i \to f$ resonance conversion transition taking account of the configuration interaction can be presented in the form

$$\Gamma_{\rm BIC}^{(i\to f)} = \mathcal{R}^{(i\to f)} \Gamma_\gamma^{(n)}, \tag{1}$$

where $\Gamma_\gamma^{(n)}$ is the radiative nuclear width, while the partial resonance conversion factor $\mathcal{R}^{(i\to f)}$ is given by[1]

$$\mathcal{R}^{(i\to f)} = \sum_\ell \frac{\alpha_d^{\tau L}(\omega_n; i \to \ell)\Gamma_\gamma(k; \ell \to f)}{2\pi[(\omega_n - \omega_\ell)^2 + (\Gamma_\ell/2)^2]}. \tag{2}$$

[1]In the present paper, all formulas are given in the relativistic units, where $\hbar = m_0 = c = 1$.

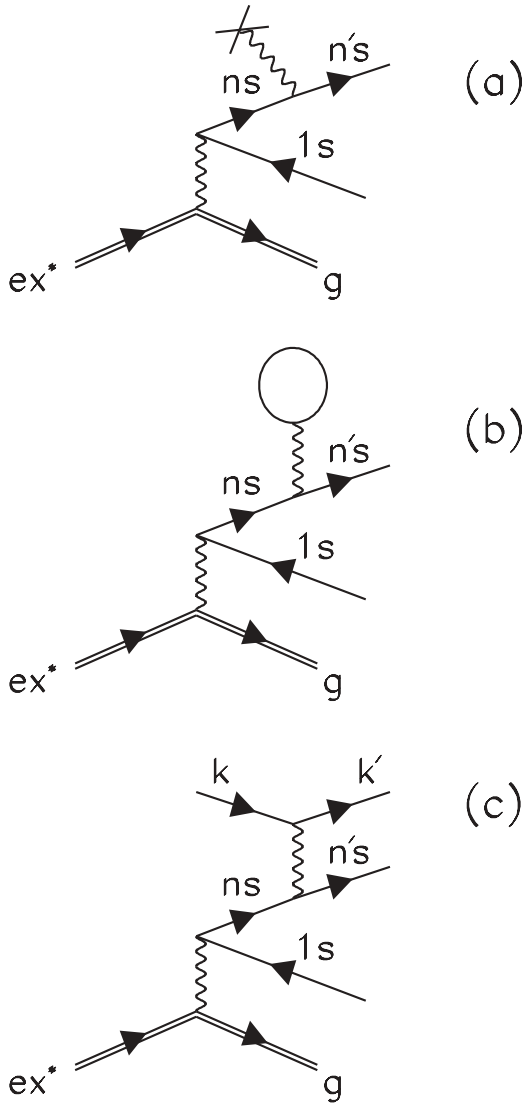

FIG. 3. Three types of interaction of the electron configurations: (a) mixing of the one-electron configurations due to the kinetic energy operator and Coulomb interaction with the nucleus, (b) one-electron mixing due to interaction with the electron core, and (c) interaction with multielectron configurations accompanied by the core excitation.

In Eqs. (1) and (2), ω_n is the nuclear transition energy, ω_ℓ is the energy of the atom in the intermediate (ℓ) state, and Γ_ℓ is the total width of the intermediate state. The total width Γ_ℓ is the sum of the natural width of the atomic level ℓ including the hole width of its decay [3] and the nuclear width if the final state of the conversion transition is not the ground one. In the case considered here, there are no holes in the intermediate state or atomic-decay channels other than the radiative one; also, nuclear widths are usually negligible compared to the atomic ones. $\Gamma_\gamma(k; \ell \to f)$ is the partial radiative width for the atomic transition $\ell \to f$ with energy k. According to the energy-conservation law, this amplitude is calculated at the emitted-photon energy

$$k = \omega_n - \omega_f, \tag{3}$$

where ω_f is the energy of the atom in the final (f) state.

TABLE I. Electron configurations of the initial Th(i), intermediate Th(ℓ), and final Th(f) states of the thorium atom in various MCDF calculations and total resonance conversion factor $\mathcal{R}$ [see Eq. (7)].

No.	Th(i) = Th(ℓ)	Th(f)	$\mathcal{R}$
1	$7s^26d^2 + 7s8s6d^2$	$7s7p6d^2 + 7s8p6d^2$	421
2	$7s^26d^2 + 7s8s6d^2 + 7s9s6d^2$	$7s7p6d^2 + 7s8p6d^2 + 7s9p6d^2$	452
3	$7s^26d^2 + 7s8s6d^2 + 7s9s6d^2 + 7s10s6d^2$	$7s7p6d^2 + 7s8p6d^2 + 7s9p6d^2 + 7s10p6d^2$	473
4	$7s^26d^2 + 7s8s6d^2 + 7s6d^3 + 8s6d^3$	$7s7p6d^2 + 7s8p6d^2 + 7p6d^3 + 8p6d^3$	1332
5	$7s^26d^2 + 7s8s6d^2 + 7s9s6d^2 + 7s10s6d^2 + 7s6d^3$	$7s7p6d^2 + 7s8p6d^2 + 7s9p6d^2 + 7s10p6d^2 + 7p6d^3$	4787
6	$7s^26d^2 + 7s8s6d^2 + 7s9s6d^2 + 7s10s6d^2 + 7s6d^3 + 8s6d^3$	$7s7p6d^2 + 7s8p6d^2 + 7s9p6d^2 + 7s10p6d^2 + 7p6d^3 + 8p6d^3$	520
7	$7s^26d^2 + 7s8s6d^2 + 7s9s6d^2 + 7s10s6d^2 + 7s6d^3 + 8s6d^3 + 9s6d^3 + 10s6d^3$	$7s7p6d^2 + 7s8p6d^2 + 7s9p6d^2 + 7s10p6d^2 + 7p6d^3 + 8p6d^3 + 9p6d^3 + 10p6d^3$	608
8	$7s^26d^2 + 7s8s6d^2 + 7s9s6d^2 + 7s10s6d^2 + 7s6d^3 + 8s6d^3 + 9s6d^3 + 10s6d^3 + 7s^25f^2 + 7s8s5f^2 + 7s9s5f^2 + 7s10s5f^2$	$7s7p6d^2 + 7s8p6d^2 + 7s9p6d^2 + 7s10p6d^2 + 7p6d^3 + 8p6d^3 + 9p6d^3 + 10p6d^3 + 7s7p5f^2 + 7s8p5f^2 + 7s9p5f^2 + 7s10p5f^2$	639

In Eq. (2), $\alpha_d^{\tau L}$ is the dimensional analog of the traditional ICC which is the ratio of the conversion and radiative widths as

$$\alpha^{\tau L} = \frac{\Gamma_c(\tau L)}{\Gamma_\gamma(\tau L)}. \tag{4}$$

Here τ and L are the type and multipolarity of the transition, respectively. The discrete conversion coefficient $\alpha_d^{\tau L}$ is calculated with the same formulas as for the usual ICC [28,35], where the continuum wave function for the conversion electron is replaced by the wave function of a discrete state. Because of the different normalization of these functions, $\alpha_d^{\tau L}$ has dimensions of energy. The relevant formulas can be found in Refs. [3,6].

Performing a summation in Eq. (1) over the final states f, we obtain the total width of the BIC decay in the form

$$\Gamma_{\mathrm{BIC}} = \mathcal{R}\Gamma_\gamma^{(n)}, \tag{5}$$

where the total resonance conversion factor

$$\mathcal{R} = \frac{\Gamma_{\mathrm{BIC}}}{\Gamma_\gamma^{(n)}} \tag{6}$$

can be written in the form

$$\mathcal{R} = \sum_f \mathcal{R}^{(i\to f)} = \sum_{f\ell} \frac{\alpha_d^{\tau L}(\omega_n; i \to \ell)\Gamma_\gamma(k; \ell \to f)}{2\pi[(\omega_n - \omega_\ell)^2 + (\Gamma_\ell/2)^2]}. \tag{7}$$

We note that $\Gamma_\ell \neq \sum_f \Gamma_\gamma(k; \ell \to f)$ by virtue of Eq. (3). It follows from Eqs. (1) and (6) that the conversion factors $\mathcal{R}^{(i\to f)}$ and $\mathcal{R}$ play the same role in BIC as ICC $\alpha^{\tau L}$ [Eq. (4)] plays in traditional conversion.

In the random-phase approximation, one can neglect interference effects in performing summation over intermediate states ℓ. Moreover, the main contribution to the total resonance conversion factor comes from a few states closest to the resonance. More detailed formulas for the transition amplitudes taking into account configuration mixing are derived in Ref. [33].

Equations (1) and (2) determine the spectrum of primary photons from resonance bridges. Ultimately, each of the f states either undergoes direct decay or decays via a conventional atomic cascade to the ground state, generating the spectrum of delayed secondary photons.

IV. RESULTS OF CALCULATIONS

A. Resonance conversion factor

The total resonance conversion factor for the $M1$ transitions from the lowest level of the initial state of the thorium atom, the respective angular momentum being $J_i = 2$, to all $J^{(\ell)}$ levels of the intermediate state was calculated within the relativistic MCDF method with regard to the Breit interaction [33]. We chose the same set of basis functions for the initial and intermediate states [see Fig. 1(b)] to meet the requirements of the completeness and orthogonality of eigenfunctions. The calculations were performed for various sets of configurations in initial (intermediate) and final states of the Th atom [below Th(i), Th(ℓ), and Th(f), respectively]. Some characteristic sets of configurations are displayed in Table I along with the values of the total conversion factor $\mathcal{R}$ obtained for them. In each set, we took into account all possible spin-orbit splittings. For example, the $7s^26d^2$ group involves three configurations as follows

$$7s^26d^2 = 7s^2_{1/2}6d^2_{3/2} + 7s^2_{1/2}6d_{3/2}6d_{5/2} + 7s^2_{1/2}6d^2_{5/2}. \tag{8}$$

Three main groups have their origins in the one-electron configurations $7s^26d^2_{3/2}$, $7s^16d^3_{3/2}$, and $7s^24f^2_{5/2}$. The first is the ground configuration for the Th atom and the other two are the lowest lying configurations of the same parity.

If the one-electron approximation is used, the only resonance electron state $8s$ makes a dominant contribution to the factor $\mathcal{R}$. The $9s$ and higher s levels may be ignored due to the large resonance defect which can be written as

$$\Delta = \omega_n - \omega_\ell. \tag{9}$$

The contribution of the d levels is modest because of the smallness of the discrete conversion coefficient α_d^{M1} for the $s \to d$ transition.

The configuration mixing gives rise to two important effects. First, the atomic levels of the Th(ℓ) state are shifted, affecting the factor $\mathcal{R}$ because of the resonance nature of the BIC process. Second, the density of the levels increases drastically. Nevertheless, only a few of the levels relating to the configuration group $7s8s6d^2$ make a main contribution to the strength of the $M1$ BIC transition. Then the levels deexcite to the $7p$ levels corresponding the $7s7p6d^2$ group. Transitions to the different p levels of the Th(f) state form

the primary photon spectrum. These are the transitions which are responsible for the isomer lifetime. The Th(f) state deexcitation into the ground Th(i) level and excited levels of the Th(ℓ) state form the secondary photon spectrum.

As mentioned before, because of the levels splitting, the conversion-transition strength is partitioned among a number of levels with specific total angular momenta. So the extension of the configuration basis leads to decreasing partial values $\mathcal{R}^{(i\to f)}$, on average, and to an increasing number of partial fragments. This explains why the factor $\mathcal{R}$ is rather stable, ranging in the majority of the cases between 421 and 639, depending on the set of configurations. Repeating the consideration of Sec. II with $\mathcal{R}\approx 600$ instead of ICC, we arrive at the lifetime of the isomer of around 4.5 min. Nevertheless, the values of $\mathcal{R}$ from MCDF calculations 4 and 5 are several times greater (see Table I). This is because of the resonance character of the effect, since, in those cases, the resonance defect Δ appears to be very small for some ℓ levels (for example, the smallest $\Delta = 0.034$ eV in calculation 5), while the discrete conversion coefficient α_d^{M1} and the radiative width Γ_γ are relatively large for these levels.

The features of ℓ levels that make a dominant contribution to $\mathcal{R}$ are presented in Table II along with the values of α_d^{M1}, Γ_γ, and the conversion factors $\mathcal{R}^{(i\to\ell)}$ for each level. The structures of the ℓ levels—that is, the fractions of configuration groups that make a sizable contribution (above about 1%) to a given level—are also displayed there. The fraction of each group was determined as the sum of squares of mixing coefficients for relativistic configurations entering into this group [see Eq. (8)]. The data in Table II are given for calculation 5, in which the value of $\mathcal{R}$ is the greatest, and for calculations 7 and 8, in which the respective values are of the same order of magnitude as in the majority of the calculations while the sets of configurations are more extensive.

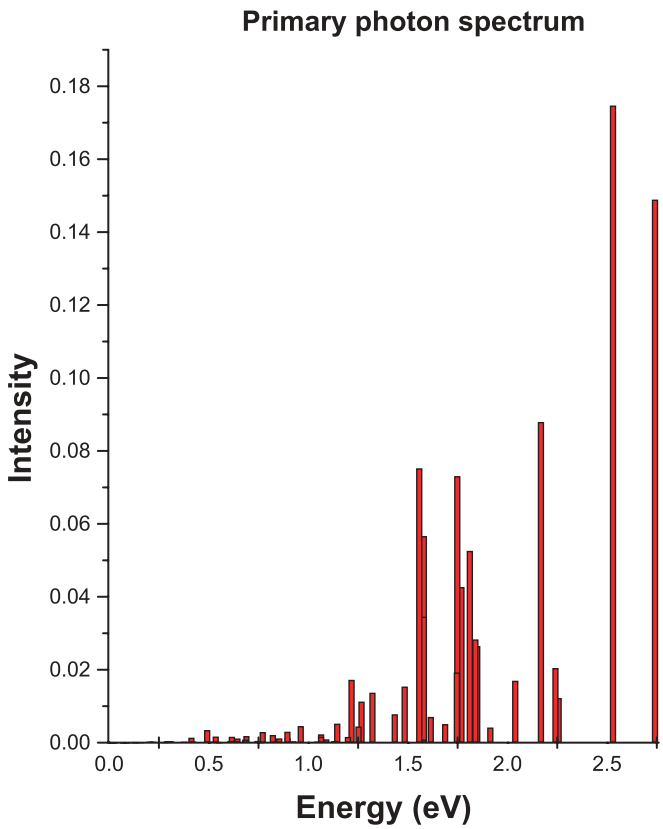

FIG. 4. (Color online) Spectrum of the primary photons.

TABLE II. Features of the ℓ-state levels that make a dominant contribution to the conversion factor $\mathcal{R}$ in the MCDF calculations 5, 7, and 8. The notation used is the following: $J^{(\ell)}$ is the angular momentum of a level, ω_ℓ is the energy of a level, α_d^{M1} is the discrete conversion coefficient for all possible $M1$ transitions $J_i \to J^{(\ell)}$, Γ_γ is the radiative width, and $\mathcal{R}^{(i\to\ell)}$ is the contribution of the level ℓ to the total conversion factor $\mathcal{R}$ [see Eq.(7)]. The decimal order of magnitudes in the fourth and fifth columns is given parenthetically. In the last column, the fraction of each group is equal to the sum of the squares of mixing coefficients for configurations entering into this group [see Eq. (8)].

No.	$J^{(\ell)}$	ω_ℓ (eV)	α_d^{M1} (eV)	Γ_γ (eV)	$\mathcal{R}^{(i\to\ell)}$	Structure of level
5	2	3.534	1.84(9)	1.55(−8)	3825	$0.60(7s8s6d^2)+0.28(7s6d^3)+0.07(7s9s6d^2)$
	3	3.252	3.36(9)	2.66(−8)	232	$0.88(7s8s6d^2)+0.11(7s6d^3)$
	2	3.467	1.68(9)	8.82(−10)	218	$0.99(7s8s6d^2)$
	1	3.062	3.36(9)	7.07(−8)	196	$1.00(7s8s6d^2)$
	2	3.150	4.00(9)	3.58(−8)	187	$0.83(7s8s6d^2)+0.16(7s6d^3)$
7	3	3.584	8.21(8)	8.47(−9)	156	$0.80(7s8s6d^2)+0.15(7s6d^3)+0.02(7s9s6d^2)$
	2	3.436	3.02(8)	1.08(−8)	128	$0.67(7s8s6d^2)+0.27(7s6d^3)+0.03(7s9s6d^2)$
	1	2.955	3.96(9)	4.46(−8)	94.6	$0.98(7s8s6d^2)$
	2	2.970	3.38(9)	3.36(−8)	64.5	$0.67(7s8s6d^2)+0.31(7s6d^3)$
	3	3.157	3.00(9)	1.48(−8)	59.9	$0.78(7s8s6d^2)+0.19(7s6d^3)$
	2	3.068	3.02(9)	1.78(−8)	45.7	$0.63(7s8s6d^2)+0.35(7s6d^3)$
	3	3.016	2.98(9)	1.62(−8)	32.8	$0.37(7s8s6d^2)+0.59(7s6d^3)$
8	3	3.325	3.70(9)	1.29(−8)	248	$0.84(7s8s6d^2)+0.11(7s6d^3)+0.02(7s8s5f^2)$
	1	3.124	3.40(9)	3.64(−8)	139	$0.96(7s8d6d^2)+0.02(7s8s5f^2)$
	2	3.221	4.16(9)	1.57(−8)	133	$0.74(7s8s6d^2)+0.22(7s6d^3)+0.01(7s8s5f^2)$
	2	3.562	9.28(7)	9.97(−9)	38.3	$0.73(7s8s6d^2)+0.20(7s6d^3)+0.01(7s8s5f^2)$
	2	3.107	1.44(9)	2.24(−8)	33.1	$0.45(7s8s6d^2)+0.51(7s6d^3)+0.01(7s^26d^2)+0.01(7s8s5f^2)$
	3	3.732	8.38(8)	5.91(−9)	14.7	$0.81(7s8s6d^2)+0.13(7s6d^3)+0.02(7s8s5f^2)+0.01(7s9s6d^2)$

TABLE III. Features of the f-state levels that make a dominant contribution to the primary photon spectrum [see Eq. (3) for the primary photon energies] in the MCDF calculations 5, 7, and 8. The notation used is the following: J_f is the angular momentum of a level, ω_f is its energy, and $\mathcal{R}^{(i\to f)}$ is the partial resonance conversion factor.

No.	J_f	ω_f (eV)	$\mathcal{R}^{(i\to f)}$	Structure of level
5	3	0.931	1046	$0.83(7s7p_{1/2}6d^2)+0.16(7s7p_{3/2}6d^2)$
	3	1.743	1023	$0.26(7s7p_{1/2}6d^2)+0.71(7s7p_{3/2}6d^2)+0.03(7p6d^3)$
	3	1.432	700	$0.77(7s7p_{1/2}6d^2)+0.20(7s7p_{3/2}6d^2)+0.02(7p6d^3)$
	2	1.309	398	$0.76(7s7p_{1/2}6d^2)+0.20(7s7p_{3/2}6d^2)+0.02(7p6d^3)$
	1	1.740	265	$0.12(7s7p_{1/2}6d^2)+0.85(7s7p_{3/2}6d^2)+0.03(7p6d^3)$
	3	2.215	233	$0.45(7s7p_{1/2}6d^2)+0.48(7s7p_{3/2}6d^2)+0.03(7p6d^3)$
	2	0.734	214	$0.92(7s7p_{1/2}6d^2)+0.06(7s7p_{3/2}6d^2)$
7	3	0.793	66.0	$0.81(7s7p_{1/2}6d^2)+0.15(7s7p_{3/2}6d^2)+0.02(7s8p6d^2)$
	2	0.591	63.5	$0.89(7s7p_{1/2}6d^2)+0.06(7s7p_{3/2}6d^2)+0.01(7p6d^3)+0.01(7s8p6d^2)$
	3	1.627	61.8	$0.25(7s7p_{1/2}6d^2)+0.67(7s7p_{3/2}6d^2)+0.03(7p6d^3)$
	2	1.717	60.5	$0.29(7s7p_{1/2}6d^2)+0.66(7s7p_{3/2}6d^2)+0.02(7p6d^3)$
	3	1.320	39.7	$0.75(7s7p_{1/2}6d^2)+0.19(7s7p_{3/2}6d^2)+0.01(7p6d^3)$
	4	1.530	32.7	$0.57(7s7p_{1/2}6d^2)+0.39(7s7p_{3/2}6d^2)+0.01(7p6d^3)+0.01(7s8p6d^2)$
	2	1.197	32.3	$0.75(7s7p_{1/2}6d^2)+0.20(7s7p_{3/2}6d^2)+0.03(7p6d^3)$
	1	1.638	27.6	$0.13(7s7p_{1/2}6d^2)+0.81(7s7p_{3/2}6d^2)+0.04(7p6d^3)$
	4	2.206	26.2	$0.40(7s7p_{1/2}6d^2)+0.44(7s7p_{3/2}6d^2)+0.11(7p6d^3)$
8	3	0.970	111.5	$0.78(7s7p_{1/2}6d^2)+0.15(7s7p_{3/2}6d^2)+0.01(7s8p6d^2)+0.02(7s7p5f^2)$
	2	0.759	95.1	$0.88(7s7p_{1/2}6d^2)+0.06(7s7p_{3/2}6d^2)+0.02(7s8p6d^2)+0.01(7p6d^3)+0.02(7s7p5f^2)$
	2	1.332	56.2	$0.73(7s7p_{1/2}6d^2)+0.20(7s7p_{3/2}6d^2)+0.02(7p6d^3)$
	4	1.943	48.0	$0.37(7s7p_{1/2}6d^2)+0.56(7s7p_{3/2}6d^2)+0.02(7p6d^3)+0.01(7s7p5f^2)$
	2	1.752	46.7	$0.37(7s7p_{1/2}6d^2)+0.53(7s7p_{3/2}6d^2)+0.02(7p6d^3)+0.01(7s7p5f^2)$
	3	1.920	36.2	$0.35(7s7p_{1/2}6d^2)+0.57(7s7p_{3/2}6d^2)+0.03(7s7p5f^2)$
	4	1.689	33.6	$0.54(7s7p_{1/2}6d^2)+0.40(7s7p_{3/2}6d^2)+0.01(7p6d^3)+0.01(7s7p5f^2)$
	3	1.731	27.2	$0.30(7s7p_{1/2}6d^2)+0.61(7s7p_{3/2}6d^2)+0.01(7p6d^3)+0.02(7s7p5f^2)$

At the same time, it follows from a comparison of the values of $\mathcal{R}^{(i\to\ell)}$ in Table II and the values of $\mathcal{R}$ in Table I that the fragmentation mentioned above is of a limited character (as might have been expected in view of the smallness of the electron-electron interaction), since, in each case, only several levels presented in Table II add up to about 96–97% of the total factor $\mathcal{R}$. Moreover, comparing the results listed in Tables II and III for sets 7 and 8 leads to an unexpected conclusion. In the more extended basis of set 8, even *stronger* concentration of the transition strength is achieved. Thus, in Table II, five states for set 7 have partial $\mathcal{R}^{i\to l}$ values that are more than 10% of the total $\mathcal{R}$ factor. Set 8 has only three such states, and they are considerably stronger. Similarly, in Table III, the corresponding numbers of states with the partial $\mathcal{R}^{i\to f}$ values more than 10% of the total $\mathcal{R}$ factor are four for set 7 and two for set 8. It specifically follows from this consideration that it would be incorrect in principle to calculate the BIC probabilities on the basis of the experimental electron-level density, as was done in Ref. [36].

The composition of levels that make a dominant contribution to $\mathcal{R}$ is determined primarily by groups of the $7s8s6d^2$ and $7s6d^3$ configurations. A considerable fraction of the $7s6d^3$ configurations (up to 59%) is explained by the inclusion of the diagonal $M1$ transitions in calculating $\mathcal{R}$ ($7s\to 7s, 6d_{3/2}\to 6d_{3/2}$, etc.). A moderate fraction ($\lesssim$7%) of the $7s9s6d^2$ configuration and a small fraction ($\lesssim$2%) of the $7s8s5f^2$ configuration are presented in some levels characterized by the largest values of $\mathcal{R}^{(i\to\ell)}$ in the most cases. Groups of configurations involving higher s states ($9s$ and $10s$) make a small contribution, but one can see from the data in Table I that their addition to Th(i), along with the addition of the corresponding groups of high p states to Th(f), may change the value of $\mathcal{R}$ significantly. This is also a manifestation of the resonance character of BIC.

We note that the lowest level in Th(i) with $J_i=2$ has the $0.98(7s^26d^2)+0.02(7s8s6d^2)$ structure in calculations 1–3, the $0.95(7s^26d^2)+0.05(7s6d^3)$ structure in calculations 4–7, and the $0.94(7s^26d^2)+0.04(7s6d^3)+0.02(7s^25f^2)$ structure in calculation 8. The structure of excited levels of the thorium atom that are the closest to the ground-state level will be discussed elsewhere. They form complexes on the basis of the $7s^26d^2$ configuration. The probabilities of the $7p\to 7s$ and $7p\to 6d$ radiative transitions are approximately identical [5]. For the sake of simplicity, we assume that the secondary decay proceeds to the ground state or the excited state closest to it (if the decay to the ground state is forbidden in the total angular momentum), this being sufficient for purposes of present-day experiments. The inclusion of decay to excited states would render the spectrum of secondary photons softer within about 0.5 eV. The structure of low-lying levels is of importance for accurately calculating the spectrum of secondary photons and for better planning and interpreting experiments (see Ref. [19] and references therein).

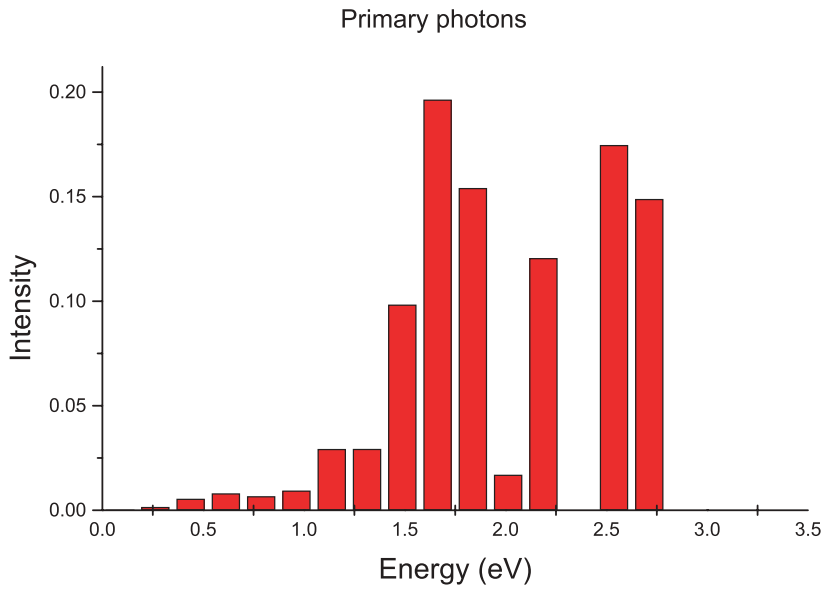

FIG. 5. (Color online) Histogram for the spectrum of the primary photons.

B. Spectra of delayed radiation

First, we calculated the spectrum of primary photons having energies k and emerging from the $i \to f$ transition [see Eqs. (1)–(3)]. It should be noted that the spectrum has nothing to do with a possible spectrum of atomic radiation. The photon energies are determined by Eq. (3) and are distinguished from energies of atomic transitions. The line intensities depend not only on radiative widths but also on the discrete conversion coefficients $\alpha_d^{\tau L}$, the low-lying $7p$ levels being predominantly populated, since the relevant probability is proportional to the cube of the transition energy. The spectrum of primary photons obtained in calculation 8 for the nuclear transition energy $\omega_n = 3.5$ eV is presented in Fig. 4.

Discussing the spectrum in Fig. 4, we note first that, as expected in the electron-bridge mechanism, there are *no* lines at the nuclear energy of 3.5 eV. The most intense lines form a doublet at the highest transition energy of 2.74 and 2.53 eV, with the total intensity of approximately 30%. As we can see in Table III, this doublet is brought about by fragmentation of the $7p_{1/2}$ state. However, another group of lines with less energy is centered around half the nuclear transition energy at ∼1–1.7 eV.

Second, we note that there are many weak lines. In view of that, the integral delayed intensity is only measured in the experiment (see, for example, Ref. [19]). Inclusion of these weak lines changes the picture significantly. To better understand the effect of the weak lines, we present the histogram of the primary photons spectrum in Fig. 5. In the histogram, one can clearly see the role of the weaker lines. The central group with the half energy appears to dominate in the integral spectrum. About 60% of the whole strength is concentrated within the range 1–2.2 eV, while ∼45% is within the range 1.4–1.8 eV.

The spectrum of the secondary photons is given in Fig. 6. The intensities of the specific lines are defined by probabilities of the f-component population, that is, by values of $\mathcal{R}^{(i\to f)}$,

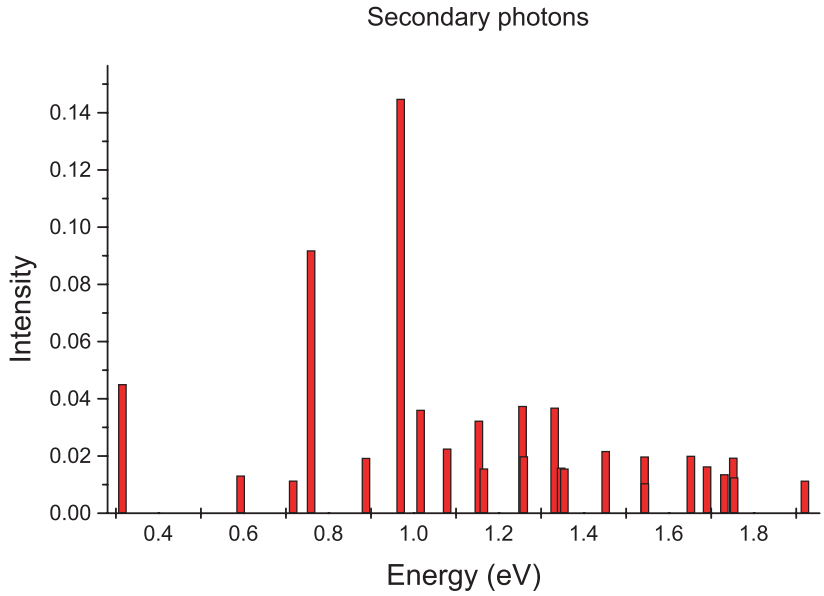

FIG. 6. (Color online) Spectrum of the secondary photons.

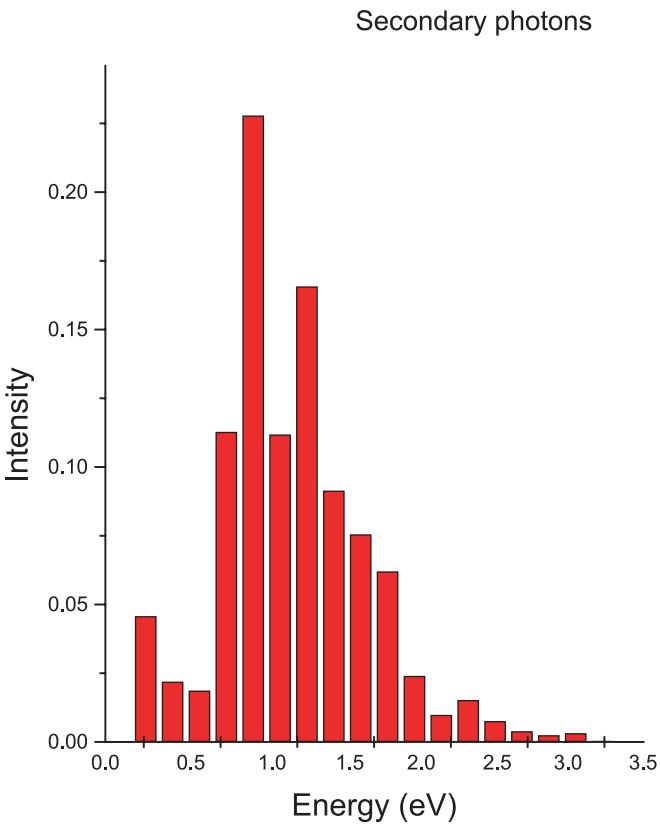

FIG. 7. (Color online) Histogram for the spectrum of the secondary photons.

together with radiative widths of transitions $f \to i$ and $f \to \ell$. Because of this, the character of the secondary photon spectrum also has nothing to do with a possible fluorescent spectrum of the atom, which is tabulated, for example, in Ref. [37]. The lines which are strong in the experimental absorption spectrum [37] in no way stand out in the spectrum in Fig. 6 and vice versa. Soft photons dominate, because primary transitions occur mainly into states near the ground one.

In finer detail, we first note that the secondary photons naturally turn out to be still softer than the primary ones. Moreover, further fragmentation of the spectrum takes place. Each state f decays into several states n. This gives rise to a great number of lines that make up the secondary spectrum, with a correspondingly lower strength of each of the lines. Nevertheless, the two strongest lines remaining have energies of 0.76 and 0.97 eV. They are complementary to the lines of 2.74 and 2.53 eV in Fig. 6 (see also Table III) and come from the succeeding decays from states populated in those transitions to the ground state. Their intensities are 9% and 14%, respectively. Therefore, the branching ratios for the decay to the ground state are 0.62 and 0.83 for those states, respectively, i.e., of the order of unity, in spite of strong fragmentation. The next most intense lines, with energies of 0.03 and 1.25 eV, are weaker by a factor of 4–5 than the strongest lines of the primary spectrum in Fig. 4. In the same way as for the primary photons spectrum, the effect of the weaker lines is shown in the relevant histogram presented in Fig. 7.

The structure of levels associated with the final state Th(f) that make a dominant contribution to the spectrum of primary photons is given in Table III for calculations 5, 7, and 8. As seen, these levels are almost completely determined by the group of $7s7p6d^2$ configurations. In this group, lower levels are dominated by the $7s7p_{1/2}6d^2$ configurations. For higher levels of this group, the fraction of the $7s7p_{3/2}6d^2$ configurations is the largest, in accordance with the fact that the $7p_{1/2}$ one-electron level lies lower than the $7p_{3/2}$ level. The fractions of the $7p6d^3$ configurations and especially the fractions of the $7s8p6d^2$ and $7s7p5f^2$ configurations are small for the majority of the levels quoted above ($\lesssim$4%). Only in the highest level at $\omega_f = 2.2$ eV from calculation 7 is the fraction of the $7p6d^3$ configurations somewhat higher, 11%. We also note several sharp peaks (three in the case of calculation 5, four in calculation 7, and two in calculation 8) and a number of less pronounced structures.

Finally, Figs. 8 and 9 present the entire spectrum of the primary and secondary photons, in which a shift of the strength toward the soft energies is readily apparent. Approximately

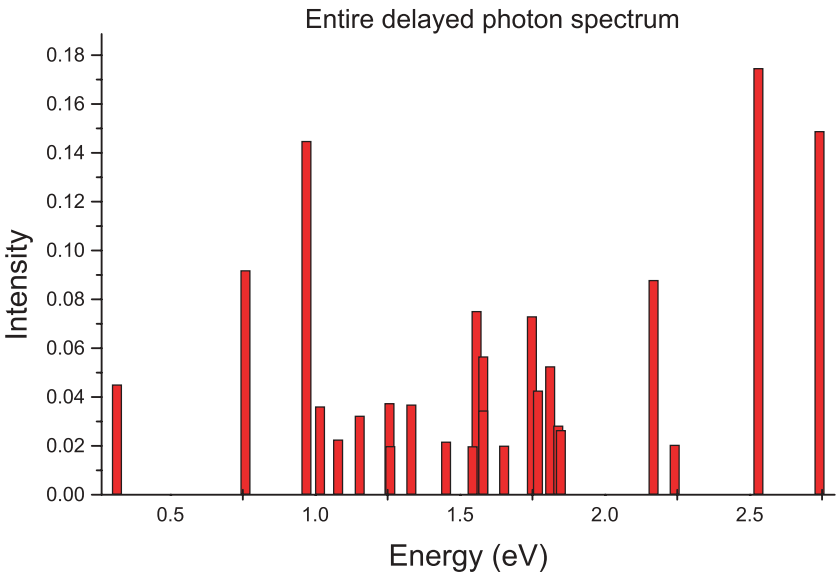

FIG. 8. (Color online) Resulting spectrum of the delayed photons.

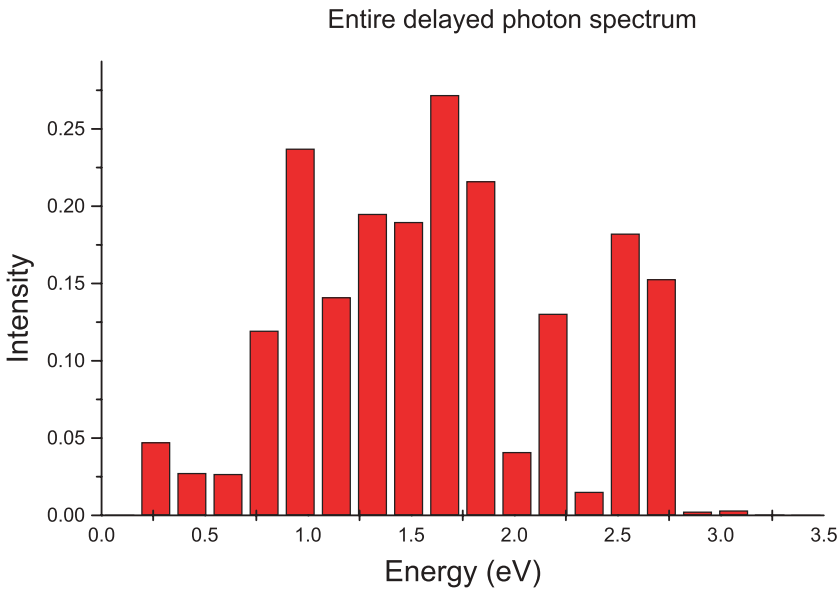

FIG. 9. (Color online) Histogram for the resulting spectrum of the delayed photons.

66% of the total strength is within 0.9–1.9 eV, and about 15% is contained only in the lines at about 2.6 eV.

Therefore, we see that the traditional channel of IC appears to be by about six orders of magnitude stronger than the BIC mechanism. We note in this connection that the previously mentioned defect of resonance even in the MCDF calculation 5, $\Delta = 0.034$ eV, remains to be large in comparison with typical line widths in the intermediate state, which are $\Gamma_\gamma \sim 10^{-8}$ eV (see Table II). On this basis, with Eq. (7) in mind, one can conclude that BIC still retains a possibility of strong potential enhancement of many orders of magnitude in the case of accidental coincidence, of the order of $\sim(\Delta/\Gamma_\gamma)^2$. This situation was considered in Ref. [19], where the low limit for the isomer lifetime of $\sim 10^{-11}$ s was obtained.

V. CONCLUSIONS

From the results presented in Sec. IV, one can see the crucial influence of the electron shell on isomer lifetime. The numerical value of the lifetime strongly depends on the energy separation E_{is} of the ground and isomeric levels with respect to the $7s$ electron binding energy, which equals 5.2 eV as mentioned above. For $E_{is} = 7.6$ eV, the most recent experimental result, the traditional channel of IC diminishes the isomer lifetime from hours to $\sim 10^{-5}$ s. Such a short lifetime makes it more difficult to measure the hyperfine splitting of the atom in the isomeric state, which measurement could be used for its direct observation [38]. The appearance of very soft conversion electrons or delayed soft radiation due to succeeding recombination in this case could give direct evidence of the deexcitation of the isomer. For $E_{is} = 3.5$ eV, the historically most referred value, the isomer decay through a BIC mechanism is realized by the numerous resonance electron bridges. These turn out to be a dominant mode. First of all, taking BIC into account reduces drastically the isomer lifetime, from several tens of hours to $\sim$5 min and less. Moreover, the isomer lifetime may diminish to a fraction of a second in the case of a random coincidence of the frequencies of the nuclear and atomic transitions.

In view of the possibility of such short lifetimes, respective experimental methods must be aimed at simultaneous measurements in the course of a permanently reproduced population of the isomer level. The use of a bulb that features a hollow cathode and in which, in the atmosphere of a buffer gas, a permanent pumping of the isomer occurs in the arc discharge within the bulb containing a $^{229}\mathrm{Th}^m$ sample seems a convenient method for this [39]. For the purpose of searching for α particles from isomer decay, it is advisable to mount a counter or the detector inlet window within the bulb itself.

Second, it becomes clear that attempts at recording a photon from a direct radiative deexcitation of the nucleus would be insufficient in relevant experimental studies. It is necessary to seek delayed photons of halved energy (see Fig. 9).

These conclusions apply to any other decay channel as well. To be more specific, we indicate that shunting the transition from the isomer to the ground state, a resonance conversion bridge complicates the observation of isomer α decay; this is because it reduces the time of accumulation of the useful spectrum, thereby dramatically lowering its statistical reliability.

The primary radiative spectrum is produced by several resonance bridge transitions to the states descended from the $7p_{1/2}$ and $7p_{3/2}$ one-electron levels. In turn, they are expected to undergo decay to the ground state with a high probability. At the same time, their energies have nothing to do with the well-known experimental spectrum [40]. Therefore, it is not advisable to try to record these particular lines in search for the isomer decay.

ACKNOWLEDGMENTS

This work was supported by the Russian Foundation for Basic Research (Project No. 05-02-17430) and the U.S. Defense Threat Reduction Agency under Contract No. DTRA 01-02-M-0534. It was also supported in part by Russian State Grant Scientific School No. 5788.2006.2.

[1] Yu. P. Gangrsky, F. F. Karpeshin, and M. B. Trzhaskovskaya, Izv. Ross. Akad. Nauk. Ser. Fiz. **68**, 149 (2004) [Bull. Russian Acad. Sci., Phys. Ser. (USA) **68**, No. 2 (2004)].
[2] F. F. Karpeshin, M. B. Trzhaskovskaya, and Yu. P. Gangrsky, Zh. Eksp. Teor. Fiz. **126**, 323 (2004) [JETP **99**, 286 (2004)].
[3] F. F. Karpeshin, M. R. Harston, F. Attallah, J. F. Chemin, J. N. Scheurer, I. M. Band, and M. B. Trzhaskovskaya, Phys. Rev. C **53**, 1640 (1996).
[4] B. A. Zon and F. F. Karpeshin, Zh. Eksp. Teor. Fiz. **97**, 401 (1990) [JETP **70**, 224 (1990)].
[5] F. F. Karpeshin, I. M. Band, M. B. Trzhaskovskaya, and B. A. Zon, Phys. Lett. **B282**, 267 (1992).
[6] F. F. Karpeshin, Phys. Part. Nuclei **37**, 522 (2006).
[7] F. F. Karpeshin, *Prompt Fission in Muonic Atoms* (Nauka, St. Petersburg, 2006).
[8] M. R. Harston, T. Carreyre, J. F. Chemin, F. F. Karpeshin, and M. B. Trzhaskovskaya, Nucl. Phys. **A676**, 143 (2000).
[9] T. Carreyre, M. R. Harston, M. Aiche *et al*., Phys. Rev. C **62**, 024311 (2000).
[10] R. G. Helmer and C. W. Reich, Phys. Rev. C **49**, 1845 (1994).
[11] C. W. Reich and R. G. Helmer, Phys. Rev. Lett. **64**, 271 (1990).
[12] Z. O. Guimarães-Filho and O. Helene, Phys. Rev. C **71**, 044303 (2005).
[13] B. R. Beck, J. A. Becker, P. Beiersdorfer, G. V. Brown, K. J. Moody, J. B. Wilhelmy, F. S. Porter, C. A. Kilbourne, and R. L. Kelley, Phys. Rev. Lett. **98**, 142501 (2007).
[14] G. M. Irwin and K. H. Kim, Phys. Rev. Lett. **79**, 990 (1997).
[15] S. B. Utter, P. Beiersdorfer, A. Barnes, R. W. Lougheed, J. R. Crespo Lopez-Urrutia, J. A. Becker, and M. S. Weiss, Phys. Rev. Lett. **82**, 505 (1999).
[16] R. W. Shaw, J. P. Young, S. P. Cooper, and O. F. Webb, Phys. Rev. Lett. **82**, 1109 (1999).
[17] D. S. Richardson, D. M. Benton, D. E. Evans, J. A. R. Griffith, and G. Tungate, Phys. Rev. Lett. **80**, 3206 (1998).
[18] Takashi T. Inamura, Phys. Scr. **71**, No. 4, C1 (2005).
[19] Yu. P. Gangrsky, V. I. Zhemenik, S. G. Zemlyanoi, F. F. Karpeshin, G. V. Myshinsky, and M. B. Trzhaskovskaya, Izv. Ross. Akad. Nauk. Ser. Fiz. **69**, 1663 (2005).
[20] F. F. Karpeshin, I. M. Band, M. B. Trzhaskovskaya, and M. A. Listengarten, Phys. Lett. **B372**, 1 (1996).
[21] F. F. Karpeshin, I. M. Band, M. B. Trzhaskovskaya, and A. Pastor, Phys. Rev. Lett. **83**, 1072 (1999).
[22] F. F. Karpeshin, Yu. N. Novikov, and M. B. Trzhaskovskaya, Yad. Fiz. **67**, 234 (2004) [Phys. At. Nucl. (USA) **67**, 217 (2004)].
[23] F. F. Karpeshin and M. B. Trzhaskovskaya. Izv. Ross. Akad. Nauk. Ser. Fiz. **67**, 1526 (2003) [Bull. Russian Acad. Sci., Phys. Ser. (USA) **67** (2003)].
[24] F. F. Karpeshin, I. M. Band, M. B. Trzhaskovskaya, and A. A. Pastor, Izv. Ross. Akad. Nauk Ser. Fiz. **63**, 38 (1999).
[25] F. F. Karpeshin, I. M. Band, and M. B. Trzhaskovskaya, Nucl. Phys. **A654**, 579 (1999).
[26] F. F. Karpeshin, I. M. Band, and M. B. Trzhaskovskaya, Zh. Eksp. Teor. Fiz. **116**, 1565 (1999) [JETP **89**, 845 (1999)].
[27] I. P. Grant, B. J. McKenzie, P. H. Norrington, D. F. Mayers, and N. C. Pyper, Comput. Phys. Commun. **21**, 207 (1980).
[28] I. M. Band, M. B. Trzhaskovskaya, C. W. Nestor Jr., P. O. Tikkanen, and S. Raman, At. Data Nucl. Data Tables **81**, 1 (2002).
[29] L. A. Sliv, Zh. Eksp. Teor. Fiz. **21**, 770 (1951).
[30] S. Raman, C. W. Nestor Jr., A. Ichihara, and M. B. Trzhaskovskaya, Phys. Rev. C **66**, 044312 (2002).
[31] N. Nica, J. C. Hardy, V. E. Iacob, S. Raman, C. W. Nestor Jr., and M. B. Trzhaskovskaya, Phys. Rev. C **70**, 054305 (2004).
[32] N. Nica, J. C. Hardy, V. E. Iacob, W. E. Rockwell, and M. B. Trzhaskovskaya, Phys. Rev. C **75**, 024308 (2007).
[33] F. F. Karpeshin and M. B. Trzhaskovskaya, Phys. At. Nucl. **69**, 571 (2006).
[34] D. F. Zaretskii and F. F. Karpeshin, Yad. Fiz. **29**, 306 (1979) [Sov. J. Nucl. Phys. **29**, 151 (1979)].
[35] I. M. Band and M. B. Trzhaskovskaya, At. Data Nucl. Data Tables **55**, 43 (1993).
[36] E. V. Tkalya, Usp. Fiz. Nauk **173**, 323 (2003).
[37] National Bureau of Standard (U.S.), atomic energy levels.
[38] B. Tordoff, T. Eronen, V. V. Elomaa *et al*., Nucl. Instrum. Methods Phys. Res. B (to be published); available from arXiv:nucl-ex/0605027.
[39] T. T. Inamura, F. F. Karpeshin, and M. B. Trzhaskovskaya, Czech. J. Phys. Suppl. B **53**, 349 (2003).
[40] A. E. Antropov, V. V. Bertsev, F. F. Karpeshin, A. A. Pastor, Yu. A. Piotrovskiy, P. Yu. Serdobintsev, I. V. Stepanov, and M. B. Trzhaskovskaya, in *Physics of Isomers, Proceedings of the First International Workshop, St. Petersburg, 2000*, edited by F. F. Karpeshin, S. N. Abramovich, and Yu. P. Gangrsky (RFNC–VNIIEF, Sarov, Russia, 2001), p. 10.